Materials Science and Engineering A 535 (2012) 306–310

Contents lists available at SciVerse ScienceDirect

Materials Science and Engineering A

journal homepage: www.elsevier.com/locate/msea

Microstructure of ultra-fine-grained high carbon steel prepared by equal channel angular pressing

Tiantian He[a], Yi Xiong[a,b,*], Fengzhang Ren[a,b], Zhiqiang Guo[a], Alex A. Volinsky[c]

[a] School of Materials Science and Engineering, Henan University of Science and Technology, Luoyang 471003, PR China
[b] Henan Key Laboratory of Advanced Non-Ferrous Metals, Luoyang 471003, PR China
[c] Department of Mechanical Engineering, University of South Florida, Tampa, FL 33620, USA

ARTICLE INFO

Article history:
Received 10 August 2011
Received in revised form 8 December 2011
Accepted 20 December 2011
Available online 27 December 2011

Keywords:
Ultra-microduplex structure
Equal channel angular pressing
Pearlitic
Microstructure

ABSTRACT

Equal channel angular pressing of a fully pearlitic Fe–0.8C steel was carried out at 923 K. The microstructure, before and after processing, was analyzed by scanning and transmission electron, and atomic force microscopy. After one pass of the equal channel angular pressing, the cementite lamellae is bent, kinked, and fractured, with its spacing significantly decreased. The shape of the local cementite is a short or elliptical bar. After four passes, an ultrafine microduplex structure (ferrite + cementite), with a grain size at the sub-micrometer level, was observed and the planar lamellae was converted to equiaxed three-dimensional grains. The cementite lamellae was fully spheroidized, with the average diameter of the cementite particle being equal to about 150 nm. Equiaxed ferrite grains, with an average size of 400 nm, are developed due to the dynamic, continuous recrystallization during the equal channel angular pressing deformation.

1. Introduction

Ultrafine grained (UFG) materials, with submicrometer grains, exhibit superior mechanical properties, as compared with conventional fine-grained materials or coarse-grained materials. Several methods have been developed to obtain UFG materials through severe plastic deformation (SPD) [1–4]. Among them, the SPD procedure of equal channel angular pressing (ECAP) is used most frequently because it has the potential for scaling up to large samples and produces reasonably homogeneous microstructures without any reduction in the cross-sectional dimensions of the samples [5]. During ECAP, the material is subjected to intense plastic straining by means of pressing a sample repeatedly through a die, containing two channels with equal cross-sections, whose intersection occurs at an angle. The sample is simply pressed through the channel and a shear strain is induced within the sample as it passes through the bending point of the channel. Repetitive pressing is feasible, as the sample's cross-section remains unchanged. A high total strain can then be achieved during a process of multiple-pass pressing [6]. Therefore, in the course of ECAP, grains are refined to the nanoscopic and sub-microcrystalline scale, which, together with dislocation hardening, results in the spectacular enhancement of the material's strength, while maintaining sufficient ductility.

High carbon steels are widely used in the industry, but they are hard to deform by SPD due to their high deformation resistance. To date, much work has been done on microstructure evolution and on the mechanical properties and fatigue behavior of UFG materials, as prepared by ECAP, including copper [7], copper-based alloys [8], aluminum and some of its alloys [9,10], magnesium alloys [11], titanium [12], middle and low carbon steels [13,14]. However, there is little information available on the grain refinement mechanism of high carbon steels. Thus, the purpose of this article is two-fold: (a) to investigate the microstructure of ECAPed UFG high carbon steels and (b) to explore the grain refinement mechanism initiated by ECAP.

2. Materials and experimental procedure

2.1. Materials

A commercial high-carbon steel (Fe–0.8 wt.%C) was used in this study. To ensure the full evolution of pearlite, and to gain different pearlite lamellae prior to ECAP, all specimens were vacuum annealed at 1273 K for 30 min and then placed into a salt bath furnace at 873 K for 30 min. This was followed by water cooling outside of the furnace.

* Corresponding author at: School of Materials Science and Engineering, Henan University of Science and Technology, Luoyang 471003, PR China.
Tel.: +86 379 64231269; fax: +86 379 64231943.
E-mail address: xy_hbdy@163.com (Y. Xiong).

0921-5093/$ – see front matter © 2011 Elsevier B.V. All rights reserved.
doi:10.1016/j.msea.2011.12.091

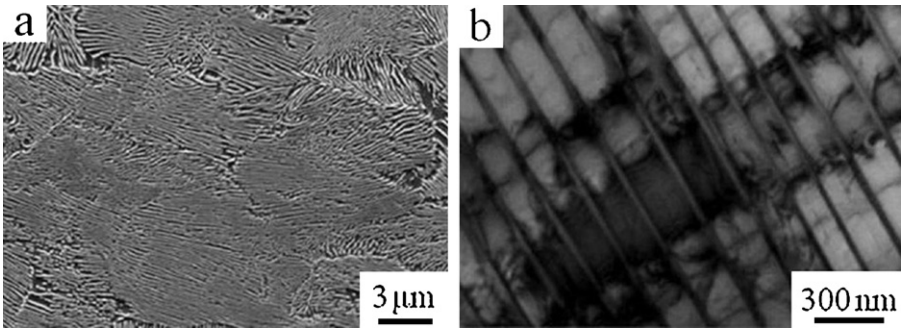

Fig. 1. Pearlite microstructure before ECAP: (a) SEM and (b) TEM.

2.2. Experimental procedure

The samples used for ECAP were cut into cylinders with 8.3 mm diameters and 49 mm lengths. The intersecting angle between the two channels was 120° and the angle of the outer arc at the intersection was 30°. Therefore, the strain per path was 0.62 [15]. The 4-pass ECAP processing was performed at 923 K. These ECAP specimens were rotated by 90° along the longitudinal axis of the specimen after each pass, in order to obtain a homogeneous microstructure. The specimen and the die were both coated with graphite and MoS_2 for lubrication, before being put in the entrance channel at the testing temperature.

The samples used for the metallographic investigation were cut from transverse cross-sections via the wire-electrode cutting method, before and after ECAP, and were then subjected to several successive steps of grinding and polishing. After that, the samples were etched in a 4 vol.% nitric acid solution, and were then characterized by a JSM-5610LV scanning electron microscope (SEM). Meanwhile, the microstructure evolution of ECAPed samples was characterized by using a JEM-2010 transmission electron microscope (TEM), operated at 200 kV. Mechanically polished, 40 μm thin foil was utilized for TEM sample preparation by using a double jet electrolytic thinning technique (30 V, 50 mA) in a 93 vol.% acetic acid/7 vol.% perchloric acid mixture. Liquid nitrogen was used for cooling during the thinning process, with the temperature raising no higher than 243 K.

The surface morphology and the three-dimensional metallography of the samples, before and after ECAP, were both observed by a P47 atomic force microscope (AFM, NT-MDT, Russia).

3. Results and discussion

3.1. Microstructure before and after ECAP

The initial microstructure of the as-received Fe–0.8 wt.%C steel is shown in Fig. 1. It can be seen that the initial microstructure was fully pearlite. The thickness of cementite lamellae is about 30 nm and the average lamellae spacing is about 150 nm, as can be seen in Fig. 1b.

Fig. 2a and b shows the SEM cross-section micrographs of the ECAPed samples after one and four passes, respectively. After one pass, the cementite lamellae shears in a regular way, with part of the lamellae being bent, kinked, and fractured. However, the lamellae are parallel to each other, as shown in Fig. 2a. After four passes, as seen in Fig. 2b, most of the original cementite lamellae disappeared and were almost completely spheroidized, with only a few lamellae still present. This is because many cementite lamellae are mainly in the bent, kinked or spheroidized forms, which coordinate the plastic deformation of the ferrite. These pearlitic phase results are comparable with the present findings. Wang et al. [16] deformed fully pearlitic steel by ECAP and also found a severe deformation of the lamellae, together with a spheroidization of the cementite lamellae. The similar results on grain refinement of carbon steel and stainless steel can be seen in Ref. [17,18], and the reason may be due to the grain refinement of surface layer generated by mechanical effect [17,19]. In addition, the effect of the deformation temperature is also significant. Wetscher et al. [20] deformed a fully pearlitic R260 steel rail by ECAP, at room temperature. After three passes, the lamellae spacing decreased significantly, but globular cementite was not found. This was most likely an effect of the elevated 923 K temperature during which this ECAP experiment was conducted. The high deformation temperature increases the diffusion capacity of the iron and carbon atoms, and thus promotes the spheroidization of the cementite. Consequently, the cementite lamellae are fully spheroidized.

The TEM microstructure, with selected-area electron diffraction (SAED) of the samples after different passes of ECAP, is shown in Fig. 3. After one pass, a marked deformation of the colonies, and an alignment of the lamellae along the pressing direction, can be seen. As can be seen in Fig. 3a, the cementite lamellae are fully fractured and then spheroidized. The shape of the cementite is a short bar or an ellipse. In this image, a significant decrease

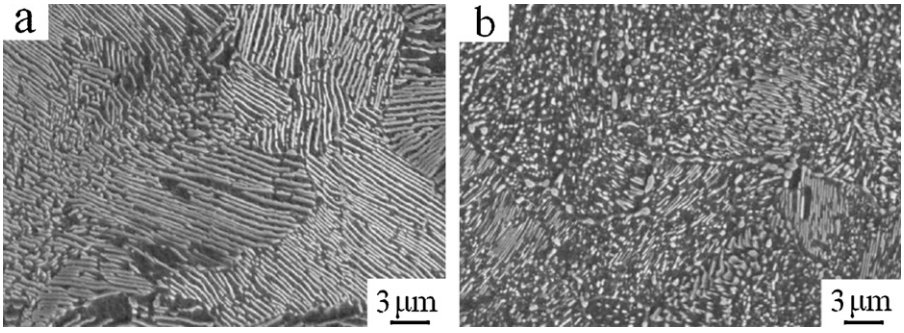

Fig. 2. SEM micrographs after different passes of ECAP: (a) one pass and (b) four passes.

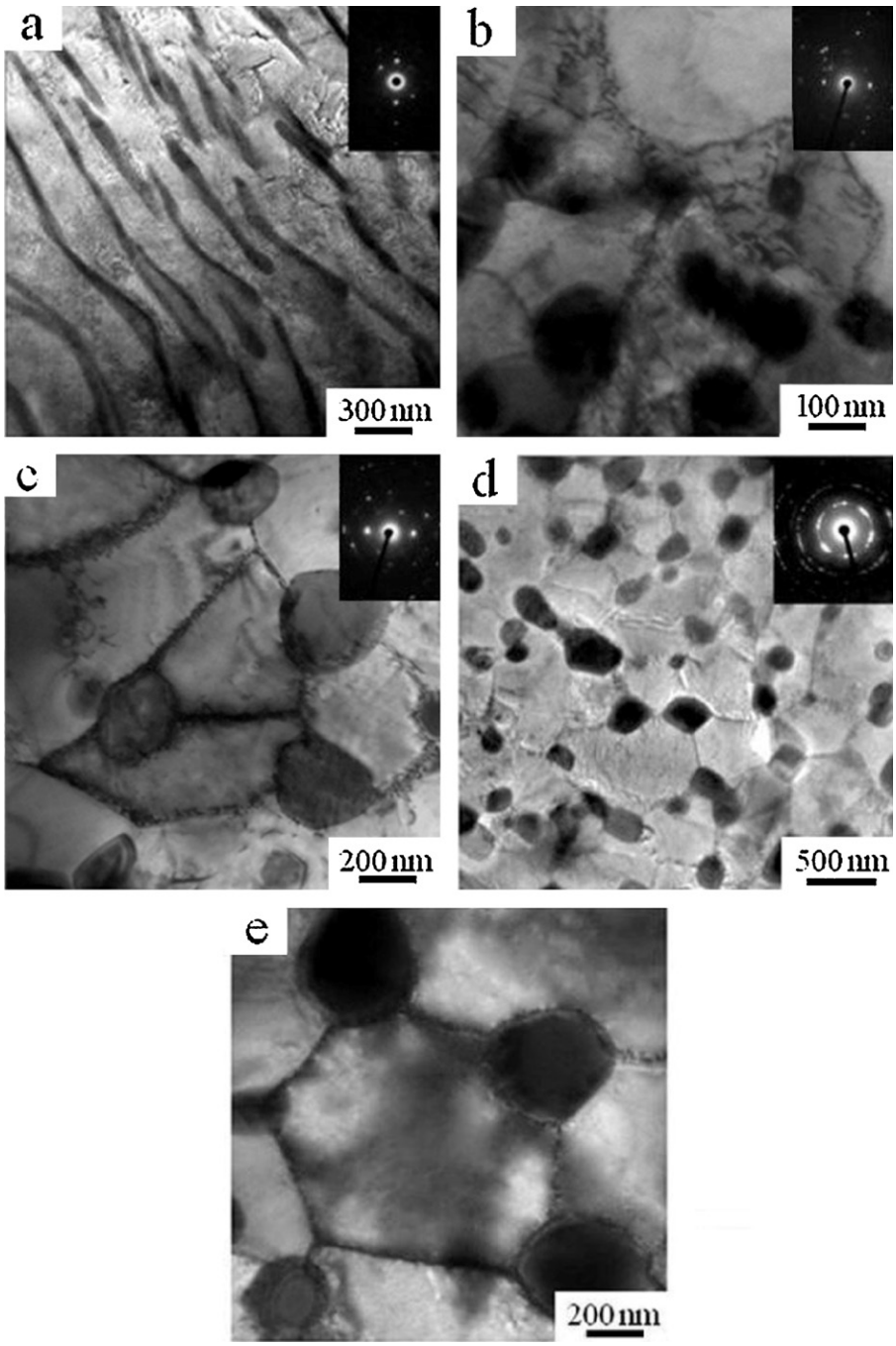

Fig. 3. TEM micrographs and the corresponding SAED patterns after different passes of ECAP: (a) one pass; (b) two passes; (c) three passes; (d) four passes; and (e) the equiaxed grain after four passes.

of the lamellae spacing is noticeable. However, the SAED pattern of Fig. 3a had relatively few diffraction spots, which suggests that the grain boundaries were mainly low-angled and that the ferrite grains were not recrystallized or refined. Fig. 3b and c is TEM micrographs, with their corresponding SAED patterns, of the sample after ECAP for two and three passes, respectively. It can be noted that the pile-up of high density dislocations, induced by severe deformation, contributes to the dislocation cells found in Fig. 3b. The formation of the dislocation cells can lead to the refinement of the ferrite grains. Meanwhile, with further increasing strains, spheroidization of the cementite lamellae is increased and most cementite lamellae are transformed to particles. After three passes, the sub-grains, with an average size of about 350 nm, developed, as shown in Fig. 3c. The original grains are subdivided by forming subgrain boundaries primarily separated by individual cells. This proves the development of arrays of high-energy, non-equilibrium boundaries. In Fig. 3b, from the corresponding SAED pattern, it is obvious that the diffraction spots have increased, which suggests that the number of the low angle boundaries have reduced. The SAED pattern of Fig. 3c consists of ring-like diffraction spots, indicating that the grain boundaries have high angular misorientation. The diffraction rings in Fig. 3c are discontinuous, which attests to the existence of low angle grain boundaries. After four passes, as seen in Fig. 3d, the cementite lamellae are fully spheroidized and the average diameter of the cementite particles is now 150 nm. The cementite particle size distribution is bimodal [21]. The formation of the bulky cementite particles, at ferrite grain boundaries, is due to the cementite lamellae spheroidization and the average

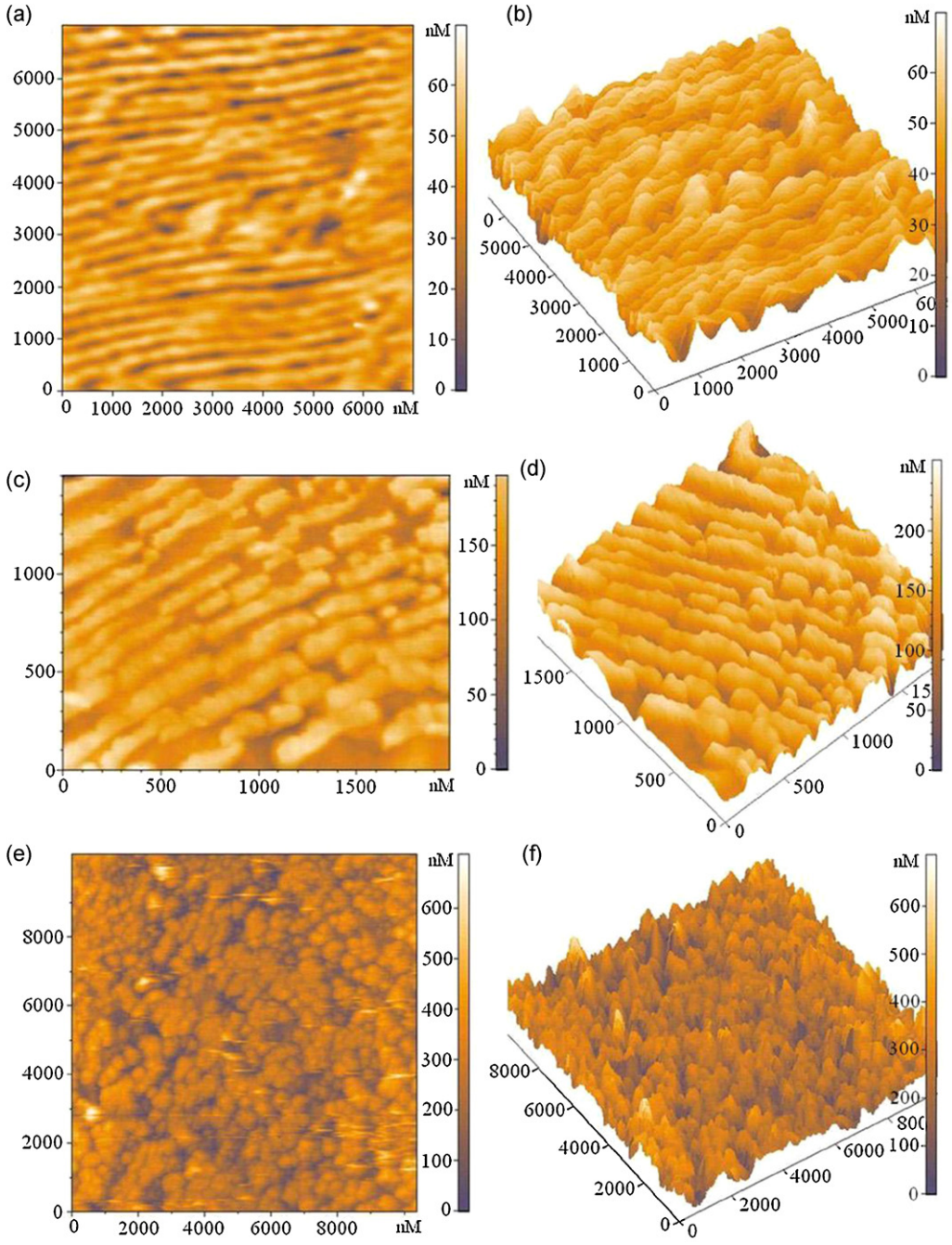

Fig. 4. AFM images of pearlite before and after ECAP: (a) planar image of the pearlite before ECAP; (b) three-dimensional image of the pearlite surface before ECAP; (c) planar image of the pearlite after one ECAP pass; (d) three-dimensional pearlite image after one ECAP pass; (e) planar pearlite image after four ECAP passes; and (f) three-dimensional pearlite image after four ECAP passes.

350 nm size of the cementite particles. Note that the size of the cementite particles inside the ferrite grain is about 90 nm. During warm deformation of ECAPed samples, many dislocations are created to accommodate the deformation between the ferrite and the cementite. The carbon atoms of the cementite then enter into the dislocations, which consequently contributes to the formation of a Cottrell atmosphere. This process can reduce the energy and thus lead to a partial dissolution of the cementite. Subsequently, dynamic recovery and dynamic recrystallization both take place, which results in a decrease of the dislocation density and the re-precipitation of the cementite inside of the ferrite matrix. Meanwhile, the ferrite grains are equiaxed, with very sharp boundaries and an average grain size of 400 nm. In Fig. 3d, the SAED pattern, with an aperture size of 2.5 μm, shows a clear and uniformly continuous diffraction ring pattern, as compared with Fig. 3c. This indicates the existence of a large number of boundaries, with high angular misorientation. Since the cementite particles in the TEM foils are too thick to obtain a diffraction pattern, almost all of the diffraction rings and spots are obtained from the ferrite. Fig. 3e shows an equiaxed ferrite grain with a typical high angle grain boundary. From Fig. 3a–d, the diffraction rings suggest that many more equiaxed structures, with high angle grain boundaries, exist in the metal as the number of ECAP passes increases to four.

During ECAP, a large strain gradient within the grain is produced by the severe plastic deformation. The distribution of dislocations thus becomes heterogeneous. Accordingly, the dislocations

are generated and accumulated in the coarse-grained material, which leads to the formation of high density tangled dislocations. With a subsequent ECAP, due to dislocation motion and interaction, the dislocations arrange themselves into dislocation walls and cells (Fig. 3b). With further straining, the dislocation cells become sharper, forming sub-grains (Fig. 3c). As there are more ECAP passes, dynamic recrystallization occurs. This is due to the high energy stored by the dislocations. Therefore, the subgrain microstructure begins to rotate independently so that more and more deformation may be accommodated. This results in the formation of new recrystallized grains, with highly misoriented boundaries (Fig. 3e). The dislocation density, however, decreases sharply at these locations. With further ECAP, dislocations are accumulated and consequently induce dynamic recrystallization. Therefore, due to dynamic continuous recrystallization, the number of the fine grains increases with the increasing number of ECAP passes and the microstructure gradually becomes homogeneous (Fig. 3d).

3.2. AFM observation

The microstructure of the sample with lamellar pearlite, before and after ECAP, was investigated by AFM as well. After ECAP, the microstructure changes from planar lamellae to three-dimensional equiaxed grains. Fig. 4a and b shows the AFM micrographs of the as-received Fe–0.8 wt.%C steel. It can be seen that the alignment of the cementite lamellae is orderly and that the lamellae are parallel to each other. This is consistent with the SEM and TEM results. The average height of the cementite lamellae is within 20 nm and can reach up to 30 nm in some places. The lamellae spacing of about 250 nm is relatively homogeneous, which is a bit higher than the SEM and TEM measurements. This is because the AFM result gives the local data, while the SEM and TEM observation gives the statistical data. The AFM images of the ECAPed sample surface, for one pass, are shown in Fig. 4c and d. After one pass, the cementite lamellae are fractured, but the alignment of the lamellae is still parallel. The same can be also seen in Figs. 2a and 3a. The height of the cementite lamellae is now about 160 nm, which is much higher than in the original state of the sample. Fig. 4e and f shows the AFM images of the ECAPed sample surface after four passes. This is similar to Figs. 2b and 3d. The cementite lamellae have completely disappeared and are fully spheroidized. The average diameter of the cementite particle is about 200 nm. Correspondingly, the height of the cementite particle is below 300 nm. The changes in height also reflect that the cementite lamellae are gradually spheroidized by increasing the number of ECAP passes. Therefore, the plastic deformation of the sample with lamellar pearlite, by ECAP, is mainly due to the deformation of the cementite lamellae.

4. Conclusions

(1) A fully pearlitic Fe–0.8 wt.%C steel was severely plastically deformed by ECAP up to a maximum of four passes, at 923 K, using route Bc. After one pass, the cementite lamellae is bent, kinked, and fractured, with the lamellae spacing decreasing significantly. The shape of the local cementite is that of a short bar or an ellipse. After four passes, the ultra-microduplex structure, with 400 nm equiaxed ferrite grains and 150 nm cementite particles, was formed.
(2) Dynamic continuous recrystallization of the ferrite, as well as spheroidization of the cementite, occurs during the deformation of ECAPed specimens at high temperatures.
(3) AFM observation showed that the microstructure changes from planar lamellae to three-dimensional equiaxed grains after four passes of ECAP and is consistent with the SEM and TEM results. The plastic deformation of the sample with lamellar pearlite, by ECAP, is mainly due to the deformation of the cementite lamellae.

Acknowledgments

The authors are grateful for Prof. G. Yang and Dr. M.X. Yang from Central Iron and Steel Research Institute for Structural Materials assistance with the ECAP work. Financial support from the National Science Foundation of China (No. 50801021) and the program for Young Key Teacher in Henan Province (Grant No. 2011GGJS-070) are also greatly appreciated.

References

[1] R.Z. Valiev, Mater. Sci. Eng. A 234–236 (1997) 59–66.
[2] R.Z. Valiev, R.K. Islamgaliev, I.V. Alexandrov, Prog. Mater. Sci. 45 (2000) 103–189.
[3] Y. Saito, H. Utsumoniya, N. Tsuji, T. Sakai, Acta Mater. 47 (1999) 579–583.
[4] M. Richert, Q. Liu, N. Hansen, Mater. Sci. Eng. A 260 (1999) 275–283.
[5] V.M. Segal, Mater. Sci. Eng. A 386 (2004) 269–276.
[6] Y. Iwahashi, Z. Horita, M. Nemoto, T.G. Langdon, Acta Mater. 46 (1998) 3317–3331.
[7] C.Z. Xu, Q.J. Wang, M.S. Zheng, J.D. Li, M.Q. Huang, Q.M. Jia, J.W. Zhu, L. Kunz, M. Buksa, Mater. Sci. Eng. A 475 (2008) 249–256.
[8] S. Qu, X.H. An, H.J. Yang, C.X. Huang, G. Yang, Q.S. Zang, Z.G. Wang, S.D. Wu, Z.F. Zhang, Acta Mater. 57 (2009) 1586–1601.
[9] M. Reihanian, R. Ebrahimi, M.M. Moshksar, D. Terada, N. Tsuji, Mater. Charact. 59 (2008) 1312–1323.
[10] S.Y. Li, Scr. Mater. 60 (2009) 356–358.
[11] A.B. Ma, J.H. Jiang, S. Naobumi, S. Ichinori, Y.C. Yuan, D.H. Yang, Y. Nishida, Mater. Sci. Eng. A 513–514 (2009) 122–127.
[12] G.I. Raab, E.P. Soshnikova, R.Z. Valiev, Mater. Sci. Eng. A 387–389 (2004) 674–679.
[13] B. Hwang, S. Lee, Y.C. Kim, N.J. Kim, D.H. Shin, Mater. Sci. Eng. A 441 (2006) 308–320.
[14] Z.Z. Du, G.H. Feng, H.G. Fu, Iron Steel 41 (2006) 74–79.
[15] Y. Iwahashi, J.T. Wang, Z. Horita, Scr. Mater. 35 (1996) 143–146.
[16] J.X. Huang, J.T. Wang, Z. Zheng, Chin. J. Mater. Res. 19 (2005) 200–206 (in Chinese).
[17] J.Z. Lu, J.W. Zhong, K.Y. Luo, L. Zhang, F.Z. Dai, K.M. Chen, Q.W. Wang, J.S. Zhong, Y.K. Zhang, Mater. Sci. Eng. A 528 (2011) 6128–6133.
[18] K.Y. Luo, J.Z. Lu, Y.K. Zhang, J.Z. Zhou, L.F. Zhang, F.Z. Dai, L. Zhang, J.W. Zhong, C.Y. Cui, Mater. Sci. Eng. A 528 (2011) 4783–4788.
[19] J.Z. Lu, K.Y. Luo, Y.K. Zhang, G.F. Sun, Y.Y. Gu, J.Z. Zhou, X.D. Ren, X.C. Zhang, L.F. Zhang, K.M. Chen, C.Y. Cui, Y.F. Jiang, A.X. Feng, L. Zhang, Acta Mater. 58 (2010) 5354–5362.
[20] F. Wetscher, R. Stock, R. Pippan, Mater. Sci. Eng. A 445–446 (2007) 237–243.
[21] W. Chen, L.F. Li, W.Y. Yang, Z.Q. Sun, Y. Zhang, Acta Metall. Sin. 45 (2009) 156–160 (in Chinese).